

# A Rule Based Segmentation Approaches to Extract Retinal Blood Vessels in Fundus Image

Md. Ahasan Kabir\*

*Department of Electronics and Telecommunication Engineering, Chittagong University of Engineering and Technology, Chittagong, Bangladesh*  
*Email: kabir.ece07@gmail.com*

## Abstract

The physiological structures of the retinal blood vessel are one of the key features that visible in the retinal images and contain the information associate with the anatomical abnormalities. It is accepted all over the world to judge the cardiovascular and retinal disease. To avoid the risk of visual impairment, appropriate vessel segmentation is mandatory. Here has proposed a segmentation algorithm that efficiently extracts the blood vessels from the retinal fundus image. The proposed segmentation algorithm is performed Lab and Principle Component (PC) based gray level conversion, Contrast Limited Adaptive Histogram Equalization (CLAHE), morphological operations, Local Property-Based Pixel Correction (LPBPC). For appropriate detection proposed vessels correction algorithm LPBPC that check the feature of the vessels and remove the wrong vessel detection. To measure the appropriateness of the proposed algorithm, the experimental results are compared with the corresponding ground truth images. The experimental results have shown that the proposed blood vessel algorithm is more accurate than the existing algorithms.

**Keywords:** Blood vessels; Segmentation; Retinopathy; CLAHE; Optical disk detection.

## 1. Introduction

Only using the retina can be the deep-rooted vessels of blood in the eye not being investigated. The main anatomical features that can be seen in the illustration of the retinal fundus are the retinal blood vessels. The structure and design reflect the effect of (cardiovascular diseases) CVDs such as cataracts, DR and high blood pressure, etc.

---

\* Corresponding author.

The destruction of the vision is the causes of cataract, glaucoma, and uncorrected refractive error, macular degeneration associated with age, diabetic retinopathy, trachoma, corneal blindness, and others. Uncorrected refractive error, cataract, and glaucoma are the main cause of blindness among the listed medical- conditions. Visualization impairment due to cataract is one of the most common reasons throughout the industrialized countries. Cataract is the most common reason for visual impairment, which account for over half of visual impairment [1]. Effective cataract diagnosis and treatment can prevent severe effects, including blindness. Cataract is a dark, cloudy region, which structures the eye lens. Cataract starts as eye proteins combine, which prevents the lens from transmitting clear image to the retina. A study indicates that the number of blind people in Europe will be about 0.075 billion by 2020 [2, 3]. The types of cataract are divided into three main categories based on the position of the retina, i.e. nuclear sclerotic, cortical, and posterior subscapular. The nuclear sclerotic is situated in the center of the lens and the lens yield a boring image. At the corner of the lens is cortical cataract, which is found in the elderly.

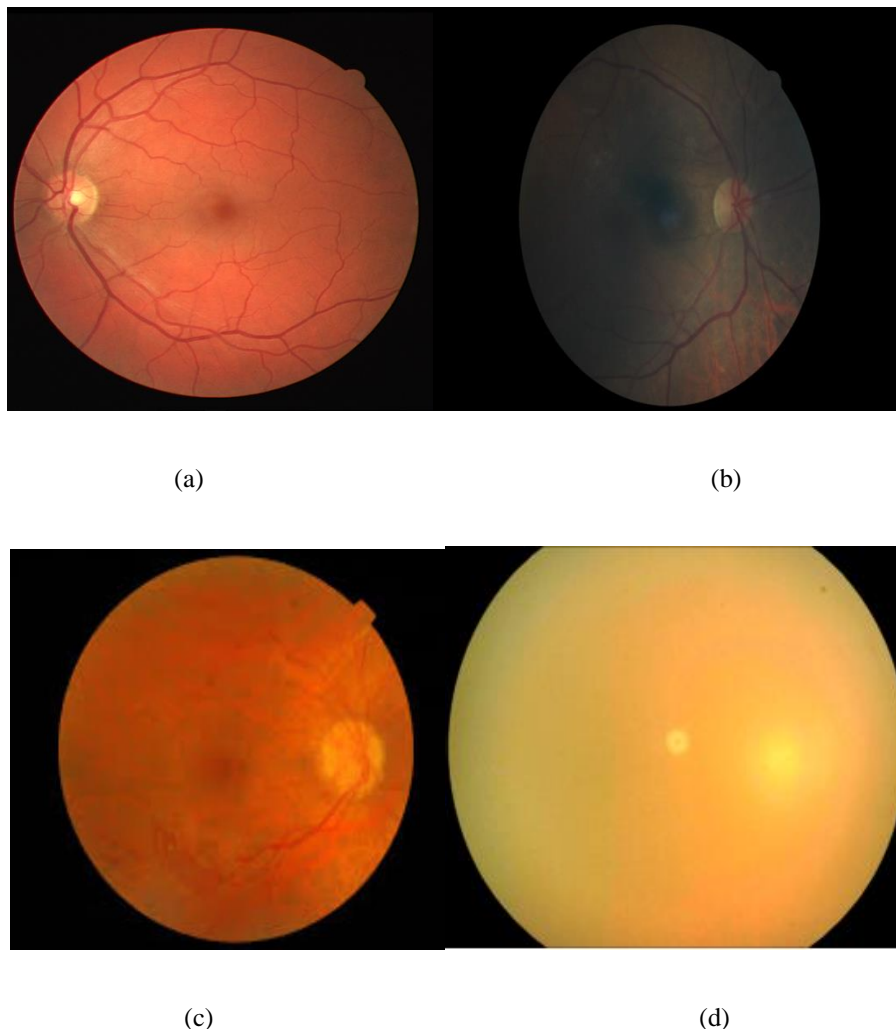


**Figure 1:** (a) Where large, small vessels and the optical disk are visible. There is very less blood vessel's data available in the mild cataract image of the eye affected in (b), While in the moderate cataract image only large blood vessels and optical discs are available in (c), and in the extreme cataract image, almost nothing can be seen in (d).

Posterior subcapsular cataracts are the severely damaging form of cataract which is situated behind the lens [4]. The majority of people aged over 40 are affected by the cataracts and this proportion is rapidly increasing over the age factor. The World Health Organization (WHO) is concerned about these increasing rates of cataract identification and diagnosis. Early diagnosis and remedy reduce the distortion and visual deterioration of cataract patients. Retinal disease can only be identified through the segmentation of the retinal vessel; however, retinal experts are required for vessel detection and segmentation. Cataracts are usually divided into four groups based on the severity, i.e. normal, moderate, mild and extreme conditions [5].

The frequency is based on the optic disk and the small or large blood vessels. The structure of the groups of cataracts is shown in the figure 1 where healthy patients without cataracts are shown clearly in figure 1(a) where large and small vessels and the optical disk are visible. There is very less blood vessel's data available in the mild cataract image of the eye affected in Figure 1 (b), while in the moderate cataract picture only large blood vessels and optical discs are available in Figure 1 (c) and in the extreme cataract image, almost nothing can be seen in Figure 1 (d). These classes of cataracts are classified as shown in Figure 1 respectively from 0 to 3. Detection and diagnosis of cataracts depend heavily on the specifics of the blood vessel and optical disk. The manual segmentation and identification of blood vessels is a very tedious process. Most vessel segmentation features include size, width, branch angle, and tortuosity that are extremely difficult for early detection and retinal disease to explore manually [6]. Also, manual segmentation takes a great deal of cost and time as it requires a segmentation system retinal eye specialist [7]. Therefore, automated extraction and segmentation of the vessels by using appropriate principles are very important for early cataract detection. In this paper, I have proposed an automated retinal blood vessel segmentation using the modified coyefilter coupled with background estimation and LPBPC approach. The contribution to segment the retinal blood vessels are as follows:

1. The proposed algorithm is the integration of the anisotropic diffusion process with the Coye filter to primarily segment the retinal blood vessels. The anisotropic diffusion process blurs the image while preserving the edge contrast. However PCA based gray level conversion contains all directional components.
2. Here, background estimation is performed using the primary segmented blood vessels, which remove the blood vessels and only represent the appropriate background. The estimated background helps to segment appropriate retinal blood vessels.
3. The low contrast vessels cannot segment without the help of local information. Here has been proposed an algorithm called LPBPC, which classifies whether a small group of pixels is blood vessels or not. This process is done based on the local contrast information.
4. Also, line features and area to perimeter ratio has been used to check the verification of blood vessels.

## **2. Related works**

Throughout the various fields of medical diagnosis, it is important to segment and examine blood vessels through imaging. Many researchers have made effective extraction and analysis algorithms. In this page, several essential contributions are summarized in the area of ophthalmology. Blood vessel segmentation can be achieved by two methods: pixel-based and pattern-based. In pixel methods, each pixel is processed to indicate

whether the vessel or background pixel is tracking correctly or not. Pixel methods use Thresholding, morphological operation and kernel recognition for filters and patterns detection. Patterns-based recognition approaches use algorithms for classifying the image of the blood vessels. Soares and his colleagues have suggested the two-dimensional (2D) Gabor wavelet transformation [8] based on supervised classification. In Ricci and his colleagues used line operators and Vector Support Machine (SVM) to segments of the blood vessels [9]. The Marin and his colleagues neural network was equipped using invariant-based features and gray-based 7D at the moment [10]. A clustering method for blood vessel segmentation based on Fuzzy C-means was proposed by Tolia and his colleagues [11]. Niemeijer and his colleagues proposed a K-Nearest Neighbor (KNN) based classification for retinal blood vessel segmentation [12]. Salem and his colleagues used a novel algorithm for blood vessel segmentation (RACAL), which is a partly supervised algorithm. Kernels are filtered for the identification of pixels of a retinal image [13]. Edge filters used the most common kernels to locate the edges in the images. Robert, Sobel, Prewitt, and Canny are the most popular kernels for edge detection. In addition, different forms of kernels can be modified to define the edges for a request. A corresponding filtering method for segmenting the blood vessel was suggested by Chaudhuri and his colleagues [14]. It used 12 templates that rotate the current template with the effect of 15 degrees. Al-Rawi and his colleagues [15] suggested a better balanced filtration system based upon Chaudhuri and his colleagues Cinsdikici and his colleagues suggested an algorithm where is used ant colony optimization matched filtering [16]. The Matched Filter-First Order Derivative of Gaussian (MF-FDOG) was proposed by Zhang and his colleagues [17]. A new fitting filter kernel for blood vessel segmentation in the retinal fundus image has been proposed for Odstrcilik and his colleagues [18]. It is used the Thresholding method to segment the bold vessel of the fundus image. Global, local, or adaptive thresholds may be used. Adaptive thresholds for segmentation are mostly used and give better performance. Hoover and his colleagues proposed a partial threshold assessment for the corresponding filter response for blood vessel segmentation [19]. Jiang and his colleagues suggested a multi-threshold testing adaptive criterion [20]. The automatic tracing algorithm for optical disc and exudate detection with fixed and variable thresholds has been proposed by Reza and his colleagues [21]. They have also discussed the use of RGB (red-blue-green) color components of fundus images for a four-sided blood vessel detection [22] algorithm. Morphological operator use mathematical operations to segment the object of interest. For image processing, there are many morphological operators. Dilation, erosion, closing, and opening [23] are the most common morphological operations. Such operators are primarily used for binary images. Nevertheless, grayscale images can also be used. For the segmentation of a visual image vasculature, Zana and his colleagues [24] employed a morphology-based approach with a cross curvature assessment. Heneghan and his colleagues [25] mixed the morphological operations of the primary and secondary vessels with the second-order derivative operator. Yang and his colleagues deployed both a fuzzy and morphological operator clustering algorithm [26]. In order to highlight the blood vessels, Mehrotra and his colleagues employed the morphologic surgeon and later the Kohonen Clustering Network applied it to the blood vessels [27]. Forward Discrete Cosine Transformation (FDCT) has been used in the improvement of image contrast followed by morphological procedures for blood vessel extraction [28]. Miri and his colleagues The morphology operator Bharkad used top hat with three different structural elements [29]. Using Gabor, Frangi and Gaussian filters, Yavuz and his colleagues [30] have increased the image of the retina, accompanied by the use of the transforming top hat and clustering method for blood vessel segments. The retinal vasculature can be segmented using the method of tracking or tracing. In

order to map the vasculature, most tracking algorithms need a seed point; the seed point depends on the performance of the algorithm. The Gaussian function was used for Gao and his colleagues [31]. With these, the blood vessels are segmented. In a three-stage recursive method, Liu and his colleagues used an adaptive tracking algorithm [32]. Delibasis and his colleagues suggested the geometric model tracking algorithm and the automated search for bifurcation of the vessel without the input of the user [33]. Vlachos and his colleagues have used a process that begins with a small group of brightness-based pixels and stops when the inter-sectorial profile is invalid [34]. The detector for the segmentation of retinal blood vessels has been proposed by Sheng and his colleagues [35]. MSST uses super pixel graph geometric structures, texture, and space data. For segmentation of the vasculature, deformable versions are also used. Espona and his colleagues used an active contour with the topological properties of the blood vessel [36]. A contour model using two pairs of active contour models for the segmenting of the blood vessels was proposed by Al-Diri and his colleagues [37]. In this way, it is used to define approximate central lines of the vessel by the generalized morphological order operator. Parallel implementation based on multi-scale functionality extraction and the region growing algorithm [38] has been proposed by Palomera-Pérez and others. At first, adaptive histogram equalization and transformation of the Gabor wavelet are used for blood vessel enhancement. Upon preprocessing, the degree and area methods of growth are implemented separately and the final outcome is achieved. The Markov Random field graph technique was used by Salazar and his colleagues for the segmentation of blood vessels and the optical disk rather than by active contour [39]. Zhao and his colleagues suggested a Lebesgue measure of  $\alpha$ -neighborhood for endless regularization of perimeters of the area with an infinite active contour [40]. In this method, regional information can also be utilized to combine intensity information with a local phase map. Gao and his colleagues proposed a completely convolutional U-shape neural network for automated segmentation technique to remove retinal vessels. For retinal fundus images, the authors used a Gaussian matched filter [41]. Li and his colleagues [42] constructed a vascular segmentation approach with multi-scaled convolutional neural networks for retinal fundus images. They also used the method of mark processing to improve segmentation precision. Dasgupta and his colleagues proposed the segmentation function of the retinal vessel to include the convolutional neural network and a hierarchical prediction as a multi-label inference task [43]. Wang and his colleagues [44] proposed cascade classification framework use computationally efficient Mahalanobis distance classifiers. Matched filter based modified Chebyshev type 1 function is used for retinal blood vessel detection in [45], also this process contains image preprocessing and post processing phase. The author in [46] proposed Gaussian match filter based preprocessing coupled with U-shaped fully convolutional neural network. This algorithm has separated the blood vessels from an inadequate contrast region. The study of literature shows that pattern and morphology-based techniques are primarily used for blood vessel segmentation. Techniques that use patterns take longer for the blood vessel classification. Morphology-based approaches are easier to calculate, but other filters require high precise segmentation of the blood vessels. Such filters depend on the morphological operation. Therefore, a hybrid segmentation approach has been attempted.

### **3. Methodology**

The proposed algorithm consists of six phases: image collection, image preprocessing and enhancement, blood vessel extraction, true/false pixel correction, optical disk detection and remove false pixel around optical disk. The block diagram of the proposed algorithm is presented in figure 2. The descriptions of the proposed

algorithm are detailed as follows:

### 3.1. Input Image Collection

The fundus retinopathy image is taken from the standard STARE and DRIVE database. The DRIVE data set has been taken from a Netherlands screening diabetic retinopathy program. The retinopathy images were taken between the ages of 25 and 90 from 400 diabetic subjects [47]. The STARE dataset also includes a number of retinal images captured by Topcon TRV 50 Fundus with a 700/605-pixel space resolution and a 24-bit gray scale resolution [48]. The sample of the DRIVE and STARE datasets image are shown in figure 3. The collections of retinal images are preprocessing using an effective filtering methodology before segment the blood vessel.

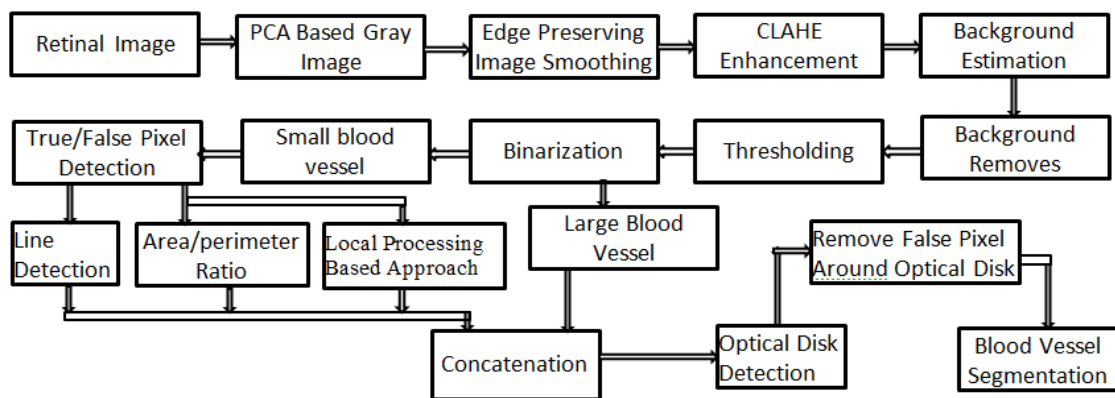


**Figure 2:** Block diagram of the proposed blood vessel segmentation algorithm.

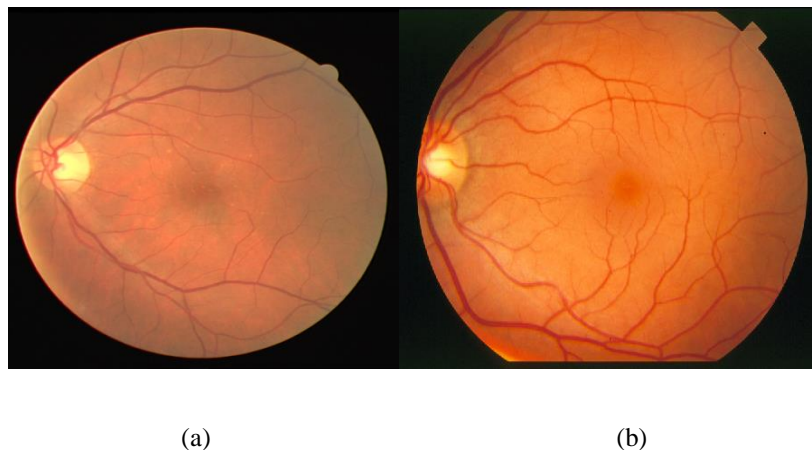


**Figure 3:** Sample images of the (a) DRIVE and (b) STARE datasets.

### 3.2. Image preprocessing and segmentation

The retinal fundus image processing are the combinations of Coye filter coupled with anisotropic diffusion based image smoothing and background estimation approach. The fundamental steps of the proposed algorithm are gray scale conversion, CLAHE based contrast enhancement, background exclusion, binarization, and small

component removal. In the beginning of the retinal fundus image, Lab color transform is done on the RGB image. Where 'L' is the representation of brightness from black (0) to white (100), 'a' represent the color space from (-) green to red (+) and 'b' from blue (-) to yellow (+). The Lab color space is closely matched with the human visual perception of lightness. The principal component analysis helps to visualize the multiple inter-correlated data. It is extract the important information from a multivariate data and express this information as a new data variable. The PCA is used to identify the direction of intensity variation in an image. The retinal fundus image contains unwanted artifacts that reduce the segmentation performance dramatically. The removal of unwanted artifacts is essential to improve the suitability of any blood vessel algorithm. The Gaussian smoothing is widely used to remove the pepper and salt image, however this process reduce the contrast intensity between blood vessel and background. To avoid the reduction of the contrast intensity, in this algorithm use anisotropic diffusion based image smoothing approach. Which improve the contrast to noise ratio while preserve the edge intensity of the blood vessels [49]. In [49] smoothing has been formulated in terms of the diffusive process. The process is iterative and the mathematical formulation can be described as

$$\frac{\partial}{\partial t} w(x, y, t) = \text{div}(c(x, y, t) \nabla w(x, y, t)) \quad (1)$$

The strength of the diffusion is controlled using  $c(x,y,t)$ . The variable  $x$  and  $y$  represent the spatial coordinates and  $t$  represents the order of the process. The image intensity  $I_{\text{gray}}(x,y,t)$  is represented by the function  $w(x,y,t)$ . The diffusion function  $c(x,y,t)$  is directly depends on the gradient of  $I_{\text{gray}}(x,y,t)$ . The  $c(x,y,t)$  is a monotonically decreasing function, which diffuse within the region and does not affect region boundaries of higher gradient. The diffusion function can be expressed as

$$c(x, y, t) = f\left(\left|\nabla I(x, y, t)\right|\right) \quad (2)$$

Then, the anisotropic diffusion based smooth image is enhanced by using CLAHE algorithm. The CLAHE is used to limit the appearance of artifact and noise in an image. Contrast can be limited by limiting the slop of the CDF function. The CLAHE enhanced image is represented by the function  $I_{\text{HE}}$  image. Now, averaging the gray scale image is to make the blur image  $I_{\text{blur}}$ . Subtract the blur image  $I_{\text{blur}}$  from the CLAHE enhanced image  $I_{\text{HE}}$  to remove the background and get the segmented image  $I_{\text{seg}}$ . Now, calculate the threshold  $T_h$  from  $I_{\text{seg}}$  image as describe in [50]. This threshold  $T_h$  is used to convert the  $I_{\text{seg}}$  image into binary image, which is the blood vessel segmented image  $I_{\text{bin}}$ . The  $I_{\text{bin}}$  contains both true and false blood vessels. This process does not fully remove the background, so here the background is estimated as follows: calculate the width  $h_w$  of the blood vessel in the horizontal direction from image  $I_{\text{bin}}$ , get two pixel  $P_2$  around the blood vessel edge. Now set a matrix with dimension  $h_w+4$  using the  $P_2$  pixels. This matrix is used to replace the corresponding intensity on the  $I_{\text{HE}}$  image. Repeat the Same process in the vertical direction and get the estimated background  $I_{\text{abg}}$ . This estimated background is used to remove the background. Image preprocessing is used to remove the unwanted artifacts from the collected retinopathy fundus retinal images. The preprocessing and segmentation approaches of the proposed algorithm are described as:

**Algorithm 1:**

1. Input retinal fundus image 'I'.
2. Convert the input RGB into  $L*a*b$  image.
3. Calculate the principal component analysis (PCA) of the input image.
4. Create a grayscale images  $I_{gray}$  based on the  $L*a*b$  image and the PCA data.
5. Smooth image by applying the anisotropic diffusion process.
6. Grayscale image is enhanced by applying the CLAHE operation. i.e.  $I_{HE} = CLAHE(I_{gray})$
7. Create a 9x9 averaging mask.
8. Create blur image  $I_{blur}$  of the grayscale image using the averaging mask.
9. Exclude background by subtraction the image  $I_{blur}$  from  $I_{HE}$  to get the segmented output  $I_{seg}$ .
10. Calculate threshold  $T_h$  using an iterative selection method.
11. Convert the  $I_{seg}$  image into binary image  $I_{bin}$  using the calculated threshold  $T_h$ .
12. To get the segmented blood vessel  $I_{sbv}$ , remove all small connected objects from  $I_{bin}$ .
13. Now using this blood vessel create an approximate background  $I_{abg}$ .
  - Find the horizontal width  $h_w$  of the blood vessel in every position where the blood vessels detected.
  - Take two horizontal pixels from both sides where the blood vessel exists.
  - Create a horizontal matrix  $h_m$  using these pixels.
  - Set the length of the horizontal matrix is  $h_w + 2.2$ .
  - Replace the corresponding horizontal image pixels with the created horizontal matrix.
  - The following steps are repeated in the vertical direction and get the approximated background image of the given fundus images.
14. Subtract the approximate background  $I_{abg}$  from the image  $I_{HE}$  and get the new segmented output  $I_{seg}$
15. Repeat steps 9-11 to get the final segmented blood vessel  $I_{sbv}$ .

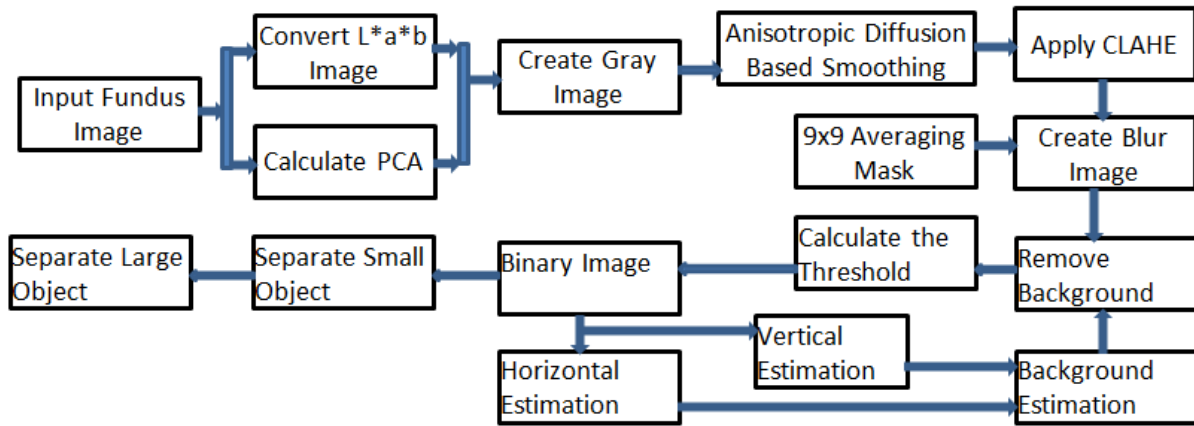
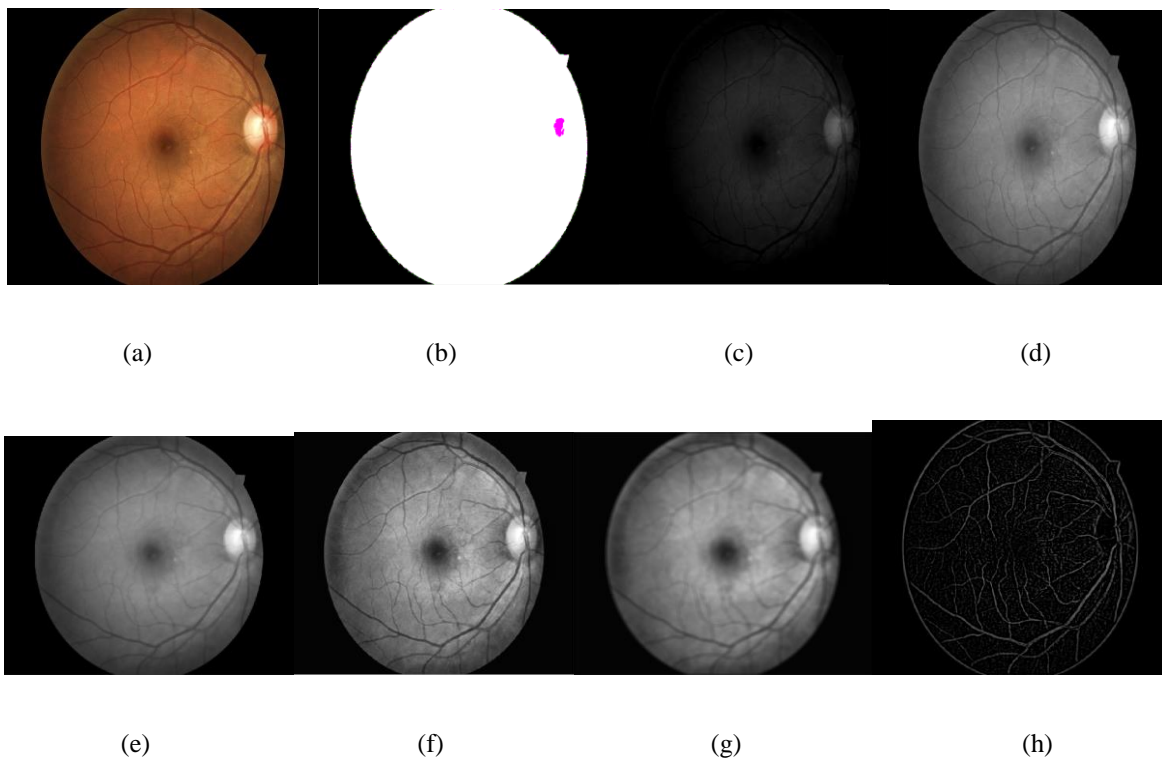


**Figure 4:** Block diagram to estimate background and blood vessels.

The small segmented blood vessels may contain true pixels or false pixels. To find the appropriateness of these pixels, here an algorithm is proposed that detect the trueness and falseness of the small blood vessels.

### 3.3. True/False pixel correction

The effectiveness of any retinal blood vessel segmentation algorithm depends on the appropriate detection of true blood vessel pixels and how suitably excludes the false pixel. To increase the effectiveness of the proposed retinal blood vessels scheme here has been proposed a correction algorithm to detect true pixels and exclude the false pixels for small separated vessels. The proposed algorithm takes the output of step 11 of algorithm 1 as an input  $I_{tf}$ . The input image  $I_{tf}$  contains both large and small connected blood vessels. Then, all small separate blood vessels  $I_{sbv}$  have been segmented. Each small segmented vessel is checked whether true/false based on



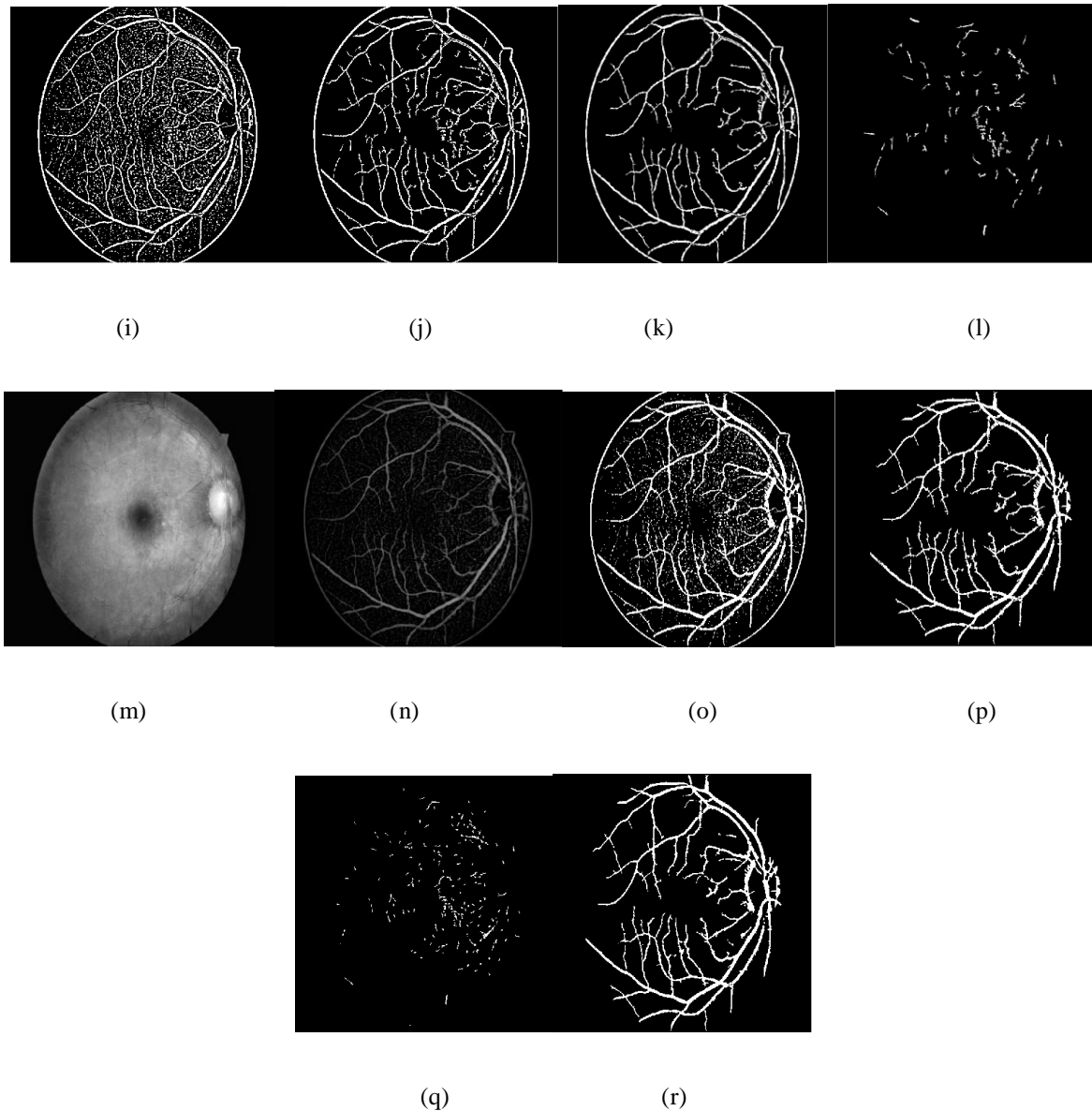


**Figure 5:** (a) Input retinal fundus image, (b) Lab image (c) PCA output (d) gray scale image (e) anisotropic diffusion based image smoothing (f) CLAHE enhanced image (g) Averaging image (h) Background Exclusion image (i) Binary image (j) remove very small separated object (k) large vessel segmented image (l) moderately small segmented object (m) estimated background (n) background Exclusion image (o) binary image of (o), (p) large blood vessels (q) Small segmented blood vessels (r) segmented blood vessel

local processing of intensity gradient and transformation based. To do so, at first the CLAHE enhanced image is cropped based on  $I_{sbv}$  by having several pixels surrounding  $I_{sbv}$ . This is called an image subblock ISC. Then, calculated the horizontal ( $h_g$ ), vertical ( $v_g$ ) and two diagonal ( $d_g$ ) intensity gradient of the  $I_{SC}$  image. The maximum intensity gradient image subblock  $I_{max\_SC}$  has been calculated from the four intensity gradient image. Then, I applied log transformation operator on  $I_{max\_SC}$  to get the transformation to image  $I_T$ . Again, the threshold value  $T_T$  is calculated by using the average of  $I_T$  plus the adjustment controller  $k$ . The value  $k$  is used to varying the threshold. Here is used an additive value  $I_{TB}$  of  $k$  and it is 10 percent of the average value. The transformed image  $I_T$  has been converted into binary image using the threshold  $T_T$ , and removed all small separate objects.

Now, a 3x3 dimensional mask is created with all elements 1 and performed hole filling operation on the  $I_{TB}$  image using the created mask. Then, the convolution operation has been performed between the mask and  $I_{TB}$  to smooth the  $I_{TB}$  image. Then performed 'AND' operation with input  $I_{sbv}$  image. If the sum is 50% of the input image  $I_{sbv}$ , marked the segmented object 'True' otherwise marked 'False'. The proposed algorithm is described as follows:

**Algorithm 2:**

1. Take the output from step 11 of algorithm 1 as the input  $I_{if}$  of this process.
2. Find all small blood vessels  $I_{sbv}$  and segment it.
3. Each segmented object is validated using intensity gradient and transformation based local processing with estimating blood vessels.

a. Get the image subblock from the CLAHE enhanced image  $I_{SC}$  such that;

$$I_{SC} = I_{CLAHE}(i, j); \text{ given that } i, j = \dim(I_{sbv}) + 3$$

b. Find the intensity gradient of  $I_{SC}$  in the horizontal  $h_g$ , vertical  $v_g$  and two diagonal  $d_g$  directions.

c. Calculate maximum intensity gradient subblock  $I_{max\_SC} = Max(h_g(i, j), v_g(i, j), d_g(i, j))$

d. Apply intensity transformation function on  $I_{max\_SC}$  image subblock such that;

$$I_T = \log_2(1 + I_{max\_SC})$$

e. Calculate threshold  $T_T = Avg(I_T) + K$ ; where k is the adjustment controller.

f. Convert  $I_T$  into binary image  $I_{TB} = \begin{cases} 1; & I_T \geq T_T \\ 0; & I_T < T_T \end{cases}$

g. Remove small separated object from the  $I_{TB}$  image.

h. Create a 3x3 mask with all elements 1.

i. Perform hole filling operation using the mask  $M_s$ .

j. Again, convolve the mask  $M_s$  with  $I_{TB}$  such that  $I_{TB}(i, j) = \begin{cases} 1 & \text{if } \left( \sum_{i,j=-1}^{i,j=1} I_{TB} * M_s \right) > 5 \\ 0 & \text{Otherwise} \end{cases}$ .

k. Perform 'AND' operation on  $I_{TB}$  and  $I_{sbv}$ .

l. If the output of step 'k' is greater than 50% of the input segmented object then detect 'true' object

otherwise detect 'false object'. i.e.  $I_{sbv} = \begin{cases} True & \text{if } (\sum I_{sbv} \cdot I_{TB}) > 50\% \text{ of } I_{sbv} \\ False & \text{Otherwise} \end{cases}$

4. Check the availability of line in the local subblock:

a. Get the image subblock as mention step 3 (a).

- b. Apply canny edge detection algorithm.
- c. Apply 'Hough transform' to find line into the image subblock.
- d. If the detected line length is greater than 60% compare with the length of the object detect 'true' otherwise detect 'false'.

5. True/false detection based on the perimeter and area of the object.

- a. Find the perimeter ( $P_o$ ) of the segmented object in terms of pixels.
- b. Find the horizontal  $h_1$ , vertical  $v_1$  and 2 diagonal  $d_1$  length.
- c. Also calculate the area ( $A_o$ ) covered by the object in terms of pixels.
- d. Calculate the ratio ( $R_o$ ) of  $A_o$  to  $P_o$ .
- e. If the output of  $R_o$  is less than 1.5 and if every length of step b is not comparable length then detect 'true' object otherwise false object.

The true and false objects can be further checked by finding the availability of line in the local subblock and compare the perimeter and area ratio of the object. To do this, the well-known 'Canny' edge detection algorithm has been performed on the ISC image. Then, I applied the 'Hough' transform to find the line into the image subblock. If the Euclidean distance of the detected line is greater than 60% of the object, marked 'True' object otherwise marked 'False' object. For the ratio of the area to the perimeter-based approach, the perimeter and area of the segmented objects are calculated in terms of pixels number. Also, the horizontal, vertical and two diagonal lengths are calculated of the object. If the ratio of the area to the perimeter is less than 1.5 and if one or two calculated lengths is 80% percent greater than the other length, then marked it 'True' blood vessel otherwise marked it 'False' blood vessel.

#### ***3.4. Detect optical disk and remove false pixel around the disk***

The presence of the optical disk influences the output of the retinal blood vessel segmentation algorithm. The optical disk is the high-intensity regions in the retinopathy images and the surrounding pixel has low intensity compared with the optical disk. These properties of the optical fundus image detect some false blood vessels around the optical disk. To remove the false pixel around the optical disk, it is essential to detect and localize optical disk in the fundus image. The input image has been blurred by applying a 9x9 averaging filter. Then, an

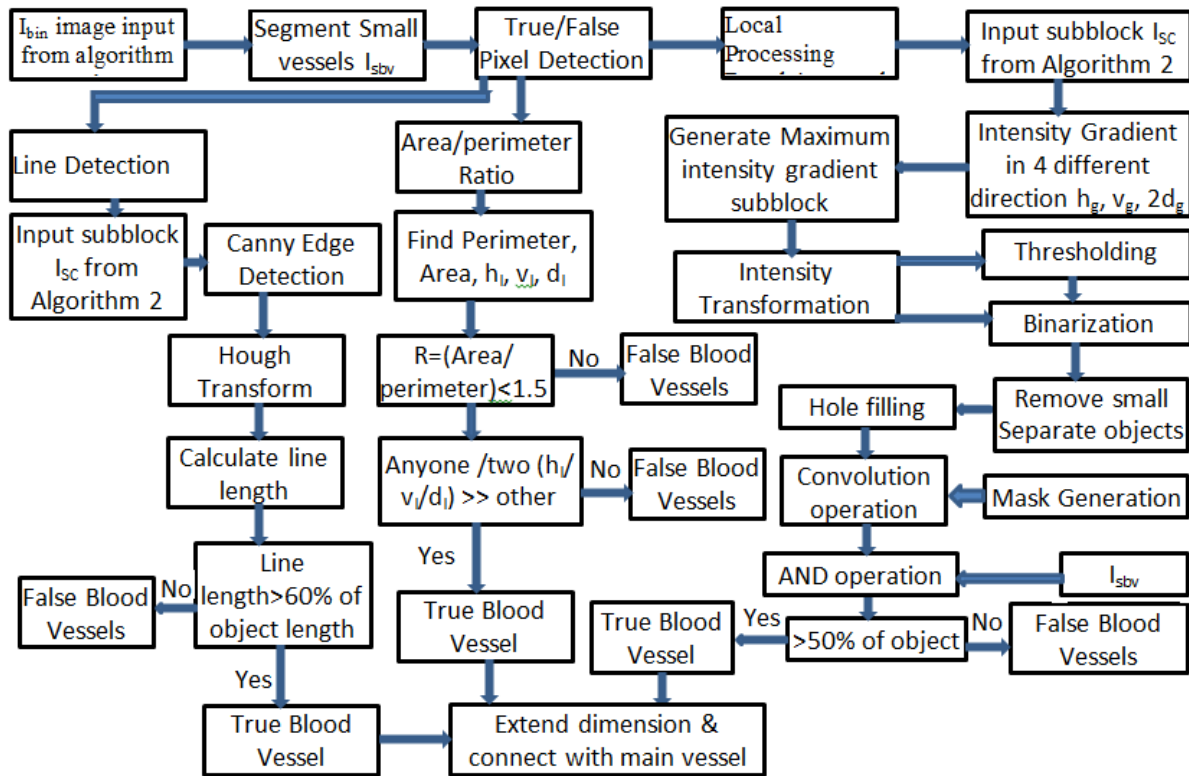


Figure 5: Block diagram to validate True/False blood vessels.

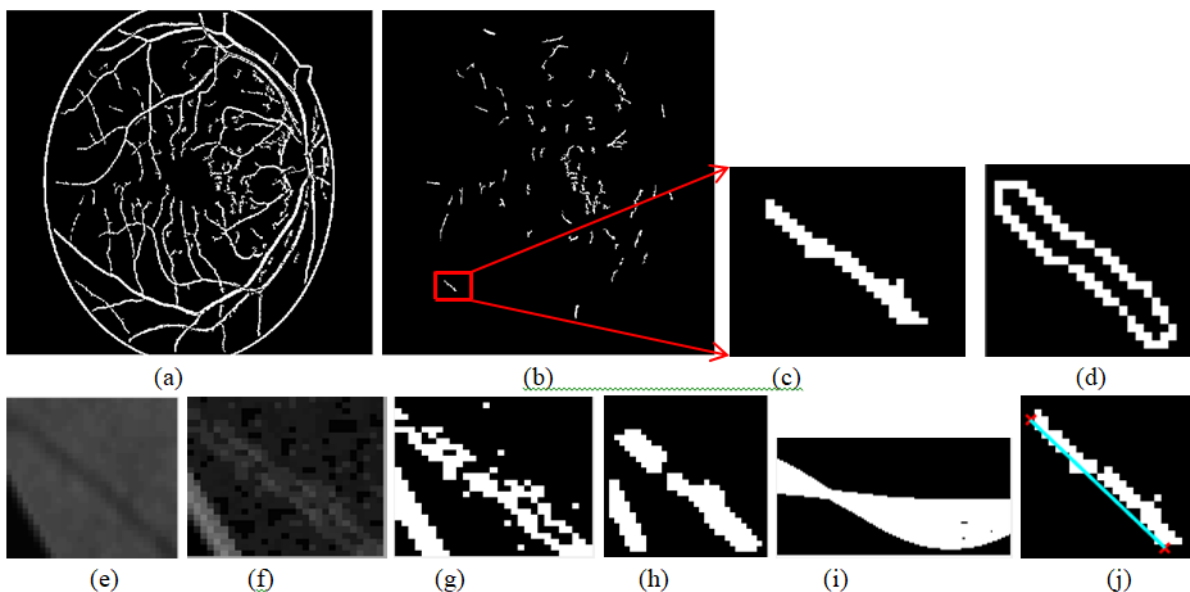


Figure 6: shown the small blood vessels validation output, (a) Blood vessel segmented output with false blood vessels (b) all small segmented blood vessel objects (c) Segmented small blood vessels for validation check (d) Perimeter of the small blood vessels (e) Region of interest (f) Intensity gradient based transformation (g) LPBPC output with small object (h) Vessels detection output of LPBPC (i) Hough transform output, (j) Hough line detection.

80x80 sliding window is used to divide the image into a subblock. Now 'C', is calculated for each channel given

$$\text{that } C = \frac{1}{1 + \sum_i (p_i - q_i)^2}.$$

Where p, q are the two subsequent image pixels. Now, all C for each channel has been combined by multiplying a constant  $t_r$ ,  $t_g$ , and  $t_b$  with corresponding red, green and blue channels. The maximum value of C is the center of the optical disk of the retinal fundus image. To remove the false pixel around the optical disk, find all pixels 'O(i,j)' within the optical disk, all pixels SO(i,j) surrounding the optical disk, and segment it from the retinal fundus image. Now, the 'SO' divided into 20x20 pixel blocks and the proposed LPBPC scheme has been applied to find blood vessels. The detection process is described in step 3 of algorithm 2. If the subblock is detected 'True' then marked each group of the pixel is true, otherwise false. These processes verify whether each pixel is situated on a blood vessel or not based on local processing. Then, all pixels situated on the boundary of the 'O' and 'SO' has been removed. Finally, the retinal blood vessel is segmented. The proposed blood vessel removal around optical disk suffers some block error. The vessel is remove block by block basis and any block may contain both true and false blood vessel. The optical disk detection, localization, and remove of false pixel algorithm are described as:

**Algorithm 3:**

1. Blur the image using a 9x9 averaging filter.
2. Use 80x80 sliding window for each blur image window.
3. Calculate  $C = \frac{1}{1 + \sum_i (p_i - q_i)^2}$  for each channel.
4. Find combined C as  $C(i, j) = t_r \times c_r + t_g \times c_g + t_b \times c_b$
5. Find the maximum value of C, which represents the center of the disk.
6. Find all pixels 'O' which is within the optical disk.
7. Find all pixels 'SO' which is surrounding the optical disk.
8. Divide the 'SO' region into 20x20 small subblocks.
9. The true vessel and false vessel detection are done of the subblock using the 3 steps of algorithm 2.
10. Remove all pixels situated on the intersecting boundary of 'O' and 'SO', except those pixels on the blood vessel.
11. Finally, the blood vessel is segmented.

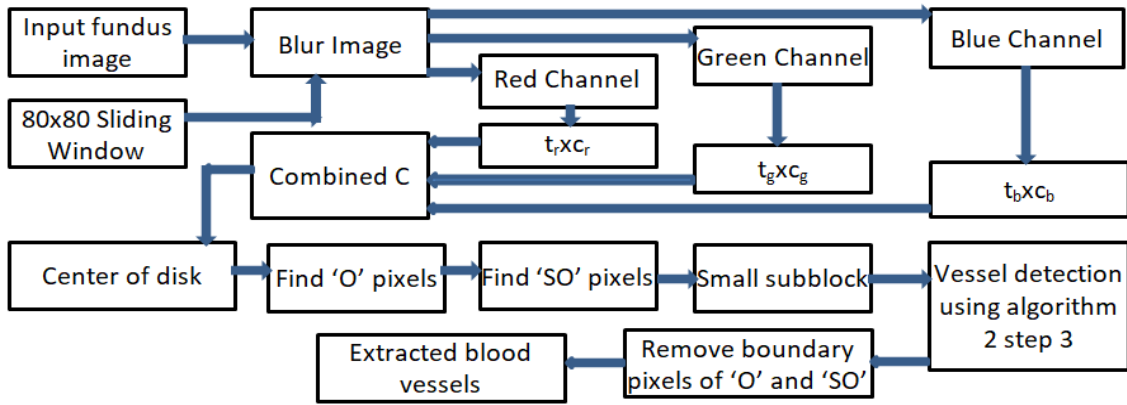


**Figure 6:** Block diagram to remove false pixels around optical disk.

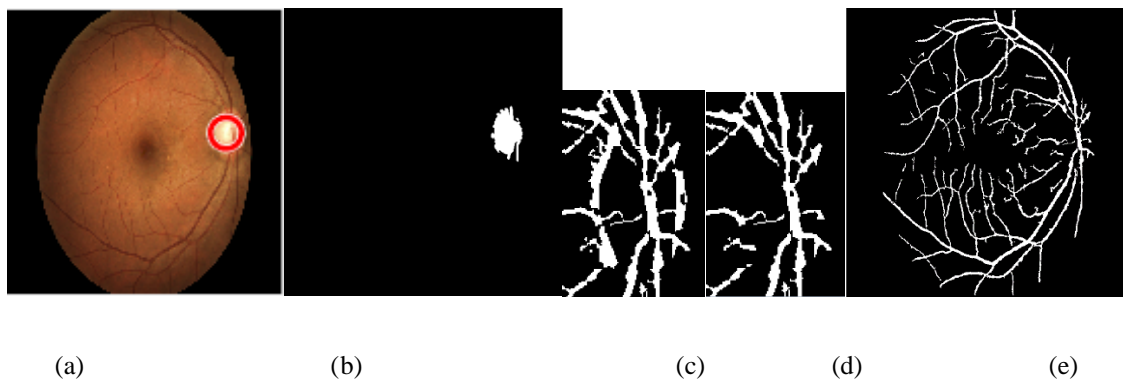


**Figure 7:** Optical disk detection and false pixel remove around optical disk. (a) Detection of optical disk (b) Optical disk segmentation (c) Detected blood vessels around optical disk (d) false pixel remove around optical disk (e) final segmented image.

#### 4. Result and Discussion

The proposed method is tested on two publicly available databases (DRIVE and STARE). Both database images contains color retinal fundus image with 8 bits color channel and have ground truth image. The effectiveness of the proposed blood vessel segmentation algorithm is measured by the parameter of Accuracy (ACC), sensitivity (Sen), Specificity (Spe). Accuracy is the ratio of the number of pixels correctly segmented from background and blood vessels to the number of pixels within the field of view (FOV). However, sensitivity and specificity represent the accuracy of blood vessel and background segmentation. Sensitivity and specificity only represent information, while accuracy is the most important performance parameter. So that, if sensitivity is high and specificity is low, which indicate that non blood vessels regions are identified as blood vessels. When sensitivity is low and specificity is high i.e., the vessels are not properly identified. When both specificity and sensitivity are high, that represent the blood vessels are properly segmented. The comparisons of blood vessel extraction in different phases are shown in figure 8.

**Table 1:** Comparison of accuracy, sensitivity, specificity and precision for different image of STARE and DRIVE dataset.

	Image no.	Before Small pixel correction				Adding true small vessels				Background estimation and addition of true vessels			
		Sen	Spe	Acc	Prec	Sen	Spe	Acc	Prec	Sen	Spe	Acc	Prec
DRIVE	21	74.59	93.62	92.20	48.56	71.14	98.62	96.57	80.68	77.79	98.13	96.61	77.06
	32	65.26	96.38	93.84	61.63	61.63	99.45	96.35	90.84	74.63	97.99	96.08	76.80
	33	68.73	95.51	93.35	57.41	65.60	99.06	96.35	85.99	73.42	98.43	96.41	80.50
	35	73.80	95.48	93.60	60.80	71.56	98.91	96.54	86.18	79.44	97.89	96.29	78.16
	40	76.51	96.44	94.93	63.81	73.47	99.11	97.17	87.11	88.80	96.43	95.85	67.07
	Average	71.78	95.49	93.58	58.44	68.68	99.03	96.60	86.16	78.82	97.77	96.25	75.92
STARE	0005	49.17	97.00	92.62	62.23	47.45	99.33	94.59	87.69	60.45	98.46	94.98	79.79
	0044	70.72	95.51	93.75	54.66	68.53	97.17	95.13	64.94	81.14	95.69	94.66	59.03
	0077	68.01	96.66	94.30	64.56	67.1	99.23	96.62	88.64	90.51	97.47	95.98	69.64
	0081	67.49	96.43	94.20	61.11	65.13	99.24	96.45	87.77	92.57	95.78	95.53	64.60
	0082	69.54	96.46	94.27	63.42	68.18	99.12	96.61	87.27	89.68	95.92	95.41	65.99
	Average	64.99	96.41	93.83	61.20	63.28	98.82	95.88	83.26	82.87	96.66	95.31	67.81

**Table 2:** Average performance parameter (accuracy, sensitivity, specificity and precision) for different vessel extraction phases.

Database	Type of phases	Sen	Spe	Prec	Acc
DRIVE	Before Small true pixel addition	63.73	96.06	62.76	93.12
	Adding true small vessels	60.64	99.37	90.86	95.88
	Background estimation and addition of true vessels	75.80	94.68	80.69	95.83
STARE	Before Small true pixel addition	61.61	96.30	58.65	93.51
	Adding true small vessels	58.79	98.95	83.97	95.71
	Background estimation and addition of true vessels	77.91	96.89	67.89	95.20

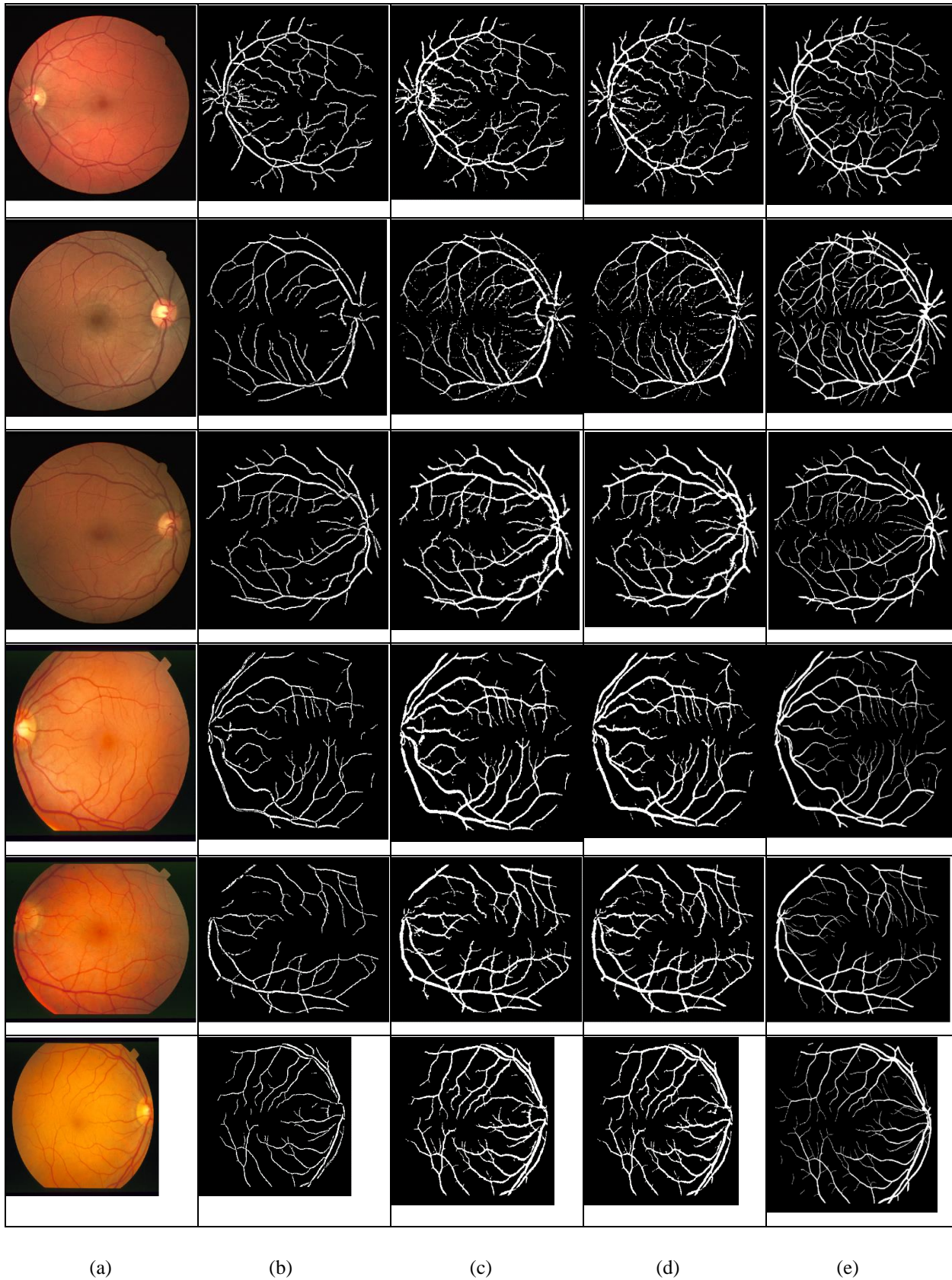


**Figure 8:** segmented blood vessel of the proposed method. (a) Input retinal fundus image, (b) initial segmented blood vessel, (c) blood vessel after background estimation and false pixel correction (d) segmented image after removing false pixel around optical disk, (e) Ground truth image.

**Table 3:** Performance comparison with other methods in terms of accuracy (%).

Year	Methods	DRIVE	STARE
	Unsupervised		
2010	Iam and his colleagues [51]	94.72	95.67
2013	Wang and his colleagues [52]	94.61	95.21
2013	Nguyen and his colleagues [53]	94.07	93.24
2014	Zhao and his colleagues [54]	94.77	95.09
2015	Yin and his colleagues [55]	94.33	93.25
2015	Azzopardi and his colleagues [56]	94.42	94.97
2016	Zhang and his colleagues [57]	94.76	95.54
2017	Rezaee and his colleagues [58]	94.63	95.21
2019	Wang and his colleagues [44]	95.41	96.40
2017	Dharmawan and his colleagues [45]	95.40	95.30
2017	Gao and his colleagues [46]	96.36	-
	Supervised		
2011	You and his colleagues [59]	94.34	94.97
2011	Marin and his colleagues [60]	94.52	95.26
2012	Fraz and his colleagues [61]	94.80	95.34
2015	Roychowdhury and his colleagues [62]	95.20	95.10
2015	Vega and his colleagues [63]	94.12	94.83
2016	Li and his colleagues [64]	95.27	96.28
2016	Liskowski and Krawiec [65]	95.15	-
2017	Barkana and his colleagues [66]	95.02	95.53
2017	Zhang and his colleagues [67]	94.66	95.47
2019	Wang and his colleagues [68]	95.36	95.38
2019	Soomro and his colleagues [69]	95.10	95.30
	Proposed Method	95.88	95.71

The inputs for different dataset are shown in figure 8(a). Figure 8(b) is the output before the true small blood vessels. The segmented blood vessels blood vessel after background estimation and false pixel correction are shown in figure 8(c). The false pixel remove around optical disk image is shown in figure 8(d) and the respective ground truth is shown in figure 8(e). The experimental result shown that, the ground truth and segmented output are closed enough in visual perception. The comparison of accuracy, specificity, sensitivity and precision for different image in DRIVE and STARE are represented in table 1. The experimental result shown that, the final segmented output have better performance parameter than the output of excluding and including small true blood vessel for both DRIVE and STARE image. The average accuracy for five Drive and STARE images are 96.25 and 95.31 when the Background is estimated and false pixel around optical disk is removed. Which is slightly less than the accuracy (96.60 and 95.88), when the background is not estimated but only adding true small vessels. However, the final output has better combination of specificity (97.77 and 96.66)

and sensitivity (78.82 and 82.87) than other. The average overall performance for DRIVE and STARE dataset are shown in table 2. It is shown that the segmented output from the phase of background estimation and addition of true vessels have higher sensitivity (75.80 and 77.91) but comparable specificity, accuracy and precision than adding true small vessel phase. However, for background estimation and addition of true vessels phase both sensitivity and specificity is high, which indicate that the blood vessels properly segmented. The comparisons of accuracy (%) with other methods are shown in table 3. The result has shown that, the accuracy (%) for Drive dataset is 95.88, which is better than [48-55, 44, 45, 59-69] and comparable with 96.36 [46]. On the other hand, the accuracy (%) for STARE dataset is 95.71 is comparable with 96.40 [44], and 96.28 [64] and better than other.

## 5. Conclusion

Retinal blood vessels segmentation helps to observe and find the retinal diseases. In this paper, I proposed a segmentation algorithm that efficiently detect and segment the retinal blood vessels. At first, the retinopathy image is de-noised using anisotropic diffusion process. Which blur the image by preserving the edge contrast. However, the blur image is enhanced using CLAHE process and estimates the background to segment the appropriate blood vessels. Background segmented image is converted into binary image using a threshold. The segmented binary image contains both small and large object, while all of the object are not desired blood vessels. To remove the false blood vessels here I have proposed Local Property Based Pixel Correction algorithm. Which identify the false object and remove from the segmented blood vessels. Moreover, to remove the false pixel around optical disk, proposed an algorithm that detects the blood vessel around optical disk and removes false pixels. The proposed algorithm is tested on different well known database (STARE, DRIVE). Experiment result shown that, the proposed retinal blood vessels algorithm have better accuracy (95.88 and 95.71) for both DRIVE and STARE dataset with compare to existing algorithm. In case of high glaucoma fundus image, it is difficult to detect retinal blood vessels. The proposed vessels algorithm is a rule based algorithm, and the classification process contains some error, which reduced the performance of the algorithm. To overcome this limitation, in future this algorithm is extended by using machine learning classifier.

## References

- [1]. D. Pascolini and S. P. Mariotti, "Global estimates of visual impairment: 2010," *British Journal of Ophthalmology*, vol. 96, no. 5, pp. 614–618, 2012.
- [2]. P. Mitchell, R. G. Cumming, K. Attebo, and J. Panchapakesan, "Prevalence of cataract in australia: the blue mountains eye study," *Ophthalmology*, vol. 104, no. 4, pp. 581–588, 1997.
- [3]. N. Congdon, J. Vingerling, B. Klein, S. West, D. Friedman, J. Kempen, B. O'Colmain, S. Wu, and H. Taylor, "Prevalence of cataract and pseudophakia/aphakia among adults in the united states." *Archives of ophthalmology (Chicago, Ill.: 1960)*, vol. 122, no. 4, pp. 487–494, 2004.
- [4]. J. J. Kanski and A. Kubicka-Trzaska, *Clinical ophthalmology: a selfassessment companion*, 1st ed. Edinburgh, New York: Elsevier Churchill Livingstone, 2007.
- [5]. J.-J. Yang, J. Li, R. Shen, Y. Zeng, J. He, J. Bi, Y. Li, Q. Zhang, L. Peng, and Q. Wang, "Exploiting ensemble learning for automatic cataract detection and grading," *Computer methods and programs in*

- biomedicine, vol. 124, pp. 45–57, 2016.
- [6]. J. A. Mobley and R. W. Brueggemeier, “Increasing the dna damage threshold in breast cancer cells,” *Toxicology and applied pharmacology*, vol. 180, no. 3, pp. 219–226, 2002.
- [7]. B. E. K. Klein, R. Klein, K. L. P. Linton, Y. L. Magli, and M. W. Neider, “Assessment of cataracts from photographs in the beaver dam eye study,” *Ophthalmology*, vol. 97, no. 11, pp. 1428–1433, 1990.
- [8]. Soares, J.V.; Leandro, J.J.; Cesar, R.M.; Jelinek, H.F.; Cree, M.J. Retinal vessel segmentation using the 2- D Gabor wavelet and, supervised classification. *IEEE Trans. Med. Imaging* 2002, 25, 1214–1222.
- [9]. Ricci, E.; Perfetti, R. Retinal blood vessel segmentation using line operators and support vector classification. *IEEE Trans. Med. Imaging* 2007, 26, 357–1365.
- [10]. Marín, D.; Aquino, A.; Gegúndez-Arias, M.E.; Bravo, J.M. A new supervised method for blood vessel segmentation in retinal images by using gray-level and moment invariants-based features. *IEEE Trans. Med. Imaging* 2011, 30, 146–158.
- [11]. Toliás, Y.A.; Panas, S.M. A fuzzy vessel tracking algorithm for retinal images based on fuzzy clustering. *IEEE Trans. Med. Imaging* 1998, 17, 263–273.
- [12]. Niemeijer, M.; Staal, J.; van Ginneken, B.; Loog, M.; Abramoff, M.D. Comparative study of retinal vessel segmentation methods on a new publicly available database. *JMI* 2004, 5370, 648–656.
- [13]. Salem, S.A.; Salem, N.M.; Nandi, A.K. Segmentation of retinal blood vessels using a novel clustering algorithm (RACAL) with a partial supervision strategy. *Med. Biol. Eng.* 2007, 45, 261–273.
- [14]. Chaudhuri, S.; Chatterjee, S.; Katz, N.; Nelson, M.; Goldbaum, M. Detection of blood vessels in retinal images using two-dimensional matched filters. *IEEE Trans. Med. Imaging* 1989, 8, 263–269.
- [15]. Al-Rawi, M.; Qutaishat, M.; Arrar, M. An improved matched filter for blood vessel detection of digital retinal images. *Comput. Biol. Med.* 2007, 37, 262–267.
- [16]. Cinsdikici, M.G.; Aydin, D. Detection of blood vessels in ophthalmoscope images using MF/ant (matched filter/ant colony) algorithm. *Comput. Methods Programs Biomed.* 2009, 96, 85–95.
- [17]. Zhang, B.; Zhang, L.; Zhang, L.; Karray, F. Retinal vessel extraction by matched filter with first-order derivative of Gaussian. *Comput. Biol. Med.* 2010, 40, 438–445.
- [18]. Odstrcilik, J.; Kolar, R.; Budai, A.; Hornegger, J.; Jan, J.; Gazarek, J.; Kubena, T.; Cernosek, P.; Svoboda, O.; Angelopoulou, E. Retinal vessel segmentation by improved matched filtering: Evaluation on a new high-resolution fundus image database. *IET Image Process.* 2013, 7, 373–383.
- [19]. Hoover, A.D.; Kouznetsova, V.; Goldbaum, M. Locating blood vessels in retinal images by piecewise threshold probing of a matched filter response. *IEEE Trans. Med. Imaging* 2000, 19, 203–210.
- [20]. Jiang, X.; Mojon, D. Adaptive local thresholding by verification-based multithreshold probing with application to vessel detection in retinal images. *IEEE Trans. Pattern Anal. Mach. Intell.* 2003, 25, 131–137.
- [21]. Reza, A.W.; Eswaran, C.; Hati, S. Automatic Tracing of Optic Disc and Exudates from Color Fundus Images Using Fixed and Variable Thresholds. *J. Med. Syst.* 2009, 33, 73, doi:10.1007/s10916-008-9166-4.
- [22]. Reza, A.W.; Eswaran, C.; Hati, S. Diabetic retinopathy: A quadtree based blood vessel detection algorithm using RGB components in fundus images. *J. Med. Syst.* 2008, 32, 147–155.
- [23]. Serra, J. *Image Analysis and Mathematical Morphology*, v. 1; Academic Press: Cambridge, MA, USA,

1982.

- [24]. Zana, F.; Klein, J.C. Segmentation of vessel-like patterns using mathematical morphology and curvature evaluation. *IEEE Trans. Image Process.* 2001, 10, 1010–1019.
- [25]. Heneghan, C.; Flynn, J.; O’Keefe, M.; Cahill, M. Characterization of changes in blood vessel width and tortuosity in retinopathy of prematurity using image analysis. *Med. Image Anal.* 2002, 6, 407–429.
- [26]. Yang, Y.; Huang, S.; Rao, N. An automatic hybrid method for retinal blood vessel extraction. *Int. J. Appl. Math. Comput. Sci.* 2008, 18, 399–407.
- [27]. Mehrotra, A.; Tripathi, S.; Singh, K.K.; Khandelwal, P. Blood Vessel Extraction for retinal images using morphological operator and KCN clustering. In *Proceedings of the 2014 IEEE International Advance Computing Conference (IACC), Gurgaon, India, 21–22 February 2014*; pp. 1142–1146, doi:10.1109/IAdCC.2014.6779487.
- [28]. Miri, M.S.; Mahloojifar, A. Retinal image analysis using curvelet transform and multistructure elements morphology by reconstruction. *IEEE Trans. Bio-Med. Eng.* 2011, 58, 1183–1192.
- [29]. Bharkad, S. Automatic segmentation of blood vessels in retinal image using morphological filters. *ICSCA 2017*, 132–136, doi:10.1145/3056662.3056710.
- [30]. Yavuz, Z.; Köse, C. Blood Vessel Extraction in Color Retinal Fundus Images with Enhancement Filtering and Unsupervised Classification. *J. Healthc. Eng.* 2017, doi:10.1155/2017/4897258.
- [31]. Gao, X.; Bharath, A.; Stanton, A.; Hughes, A.; Chapman, N.; Thom, S. A method of vessel tracking for vessel diameter measurement on retinal images. In *Proceedings of the 2001 International Conference on Image Processing (Cat. No.01CH37205), Thessaloniki, Greece, 7–10 October 2001*; Volume 2, pp. 881–884.
- [32]. Liu, I.; Sun, Y. Recursive tracking of vascular networks in angiograms based on the detection-deletion scheme. *IEEE Trans. Med. Imaging* 1993, 12, 334–341.
- [33]. Delibasis, K.K.; Kechriniotis, A.I.; Tsonos, C.; Assimakis, N. Automatic model-based tracing algorithm for vessel segmentation and diameter estimation. *Comput. Methods Programs Biomed.* 2010, 100, 108–122.
- [34]. Vlachos, M.; Dermatas, E. Multi-scale retinal vessel segmentation using line tracking. *Comput. Med. Imaging Graph.* 2010, 34, 213–227.
- [35]. Sheng, B.; Li P.; Mo, S.; Li, H.; Hou, X.; Wu, Q.; Qin, J.; Fang, R.; Feng, D.D. Retinal Vessel Segmentation Using Minimum Spanning Superpixel Tree Detector. *IEEE Trans. Cybern.* 2018, 1–13, doi:10.1109/TCYB.2018.2833963.
- [36]. Espona, L.; Carreira, M.J.; Penedo, M.G.; Ortega, M. Retinal vessel tree segmentation using a deformable contour model. In *Proceedings of the 2008 19th International Conference on Pattern Recognition, Tampa, FL, USA, 8–11 December 2008*; pp. 1-4.
- [37]. Al-Diri, B.; Hunter, A.; Steel, D. An active contour model for segmenting and measuring retinal vessels. *IEEE Trans. Med. Imaging* 2009, 28, 1488–1497.
- [38]. Palomera-Pérez, M.A.; Martínez-Pérez, M.E.; Benítez-Pérez, H.; Ortega-Arjona, J.L. Parallel multiscale feature extraction and region growing: Application in retinal blood vessel detection. *IEEE Trans. Inf. Technol. Biomed.* 2010, 14, 500–506.
- [39]. Salazar-Gonzalez, A.; Kaba, D.; Li, Y.; Liu, X. Segmentation of the blood vessels and optic disk in

- retinal images. *IEEE J. Biomed. Health Inform.* 2014, 18, 1874–1886.
- [40]. Zhao, Y.; Rada, L.; Chen, K.; Harding, S.P.; Zheng, Y. Automated Vessel Segmentation Using Infinite Perimeter Active Contour Model with Hybrid Region Information with Application to Retinal Images. *IEEE Trans. Med. Imaging* 2015, 34, 1797–807.
- [41]. Gao, X.; Cai, Y.; Qiu, C.; Cui, Y. Retinal blood vessel segmentation based on the Gaussian matched filter and U-net. In *Proceedings of the 2017 10th International Congress on Image and Signal Processing, BioMedical Engineering and Informatics (CISP-BMEI), Shanghai, China, 14–16 October 2017*; pp. 1–5.
- [42]. Li, M.; Yin, Q.; Lu, M. Retinal Blood Vessel Segmentation Based on Multi-Scale Deep Learning. In *Proceedings of the 2017 10th International Congress on Image and Signal Processing, BioMedical Engineering and Informatics (CISP-BMEI), Shanghai, China, 14–16 October 2017*.
- [43]. Dasgupta, A.; Singh, S. A fully convolutional neural network based structured prediction approach towards the retinal vessel segmentation. In *Proceedings of the 2017 IEEE 14th International Symposium on Biomedical Imaging (ISBI 2017), Melbourne, VIC, Australia, 18–21 April 2017*; pp. 248–251.
- [44]. X. Wang, X. Jiang, J. Ren, 'Blood vessel segmentation from fundus image by a cascade classification framework,' *Pattern Recognition* 88 (2019) 331–341.
- [45]. D. A. Dharmawan and B. P. Ng, "A new two-dimensional matched filter based on the modified chebyshev type i function for retinal vessels detection," in *Engineering in Medicine and Biology Society (EMBC), 2017 39th Annual International Conference of the IEEE. IEEE, 2017*, pp. 369–372.
- [46]. X. Gao, Y. Cai, C. Qiu, and Y. Cui, "Retinal blood vessel segmentation based on the gaussian matched filter and u-net," in *Image and Signal Processing, BioMedical Engineering and Informatics (CISP-BMEI), 2017 10th International Congress on. IEEE, 2017*, pp. 1–5.
- [47]. Staal J, Abràmoff MD, Niemeijer M, Viergever MA, Van Ginneken B (2004) Ridge-based vessel segmentation in color images of the retina. *IEEE Trans Med Imaging* 23:501–509
- [48]. Hoover A, Goldbaum M (2003) Locating the optic nerve in a retinal image using the fuzzy convergence of the blood vessels. *IEEE Trans Med Imaging* 22:951–958
- [49]. Gerig, Guido, et al. "Nonlinear anisotropic filtering of MRI data", *IEEE Transactions on medical imaging* 11.2 (1992), 221-232.
- [50]. A. Hoover, V. Kouznetsova and M. Goldbaum, "Locating Blood Vessels in Retinal Images by Piece-wise Threhsold Probing of a Matched Filter Response", *IEEE Transactions on Medical Imaging*, vol. 19 no. 3, pp. 203-210, March 2000
- [51]. B. Lam, Y.G.A. Liew, General retinal vessel segmentation using regularization-based multiconcavity modeling, *IEEE Trans. Med. Imaging* 29 (7) (2010) 1369–1381.
- [52]. Y. Wang, G. Ji, P. Lin, E. Trucco, Retinal vessel segmentation using multiwavelet kernels and multiscale hierarchical decomposition, *Pattern Recognit.* 46 (8) (2013) 2117–2133.
- [53]. U.T. Nguyen, A. Bhuiyan, L.A. Park, K. Ramamohanarao, An effective retinal blood vessel segmentation method using multi-scale line detection, *Pattern Recognit.* 46 (3) (2013) 703–715.
- [54]. Y.Q. Zhao, X.H. Wang, X.F. Wang, F.Y. Shih, Retinal vessels segmentation based on level set and region growing, *Pattern Recognit.* 47 (7) (2014) 2437–2446.

- [55]. B. Yin , H. Li , B. Sheng , X. Hou , Y. Chen , W. Wu , P. Li , R. Shen , Y. Bao , W. Jia , Vessel extraction from non-fluorescein fundus images using orientation-aware detector, *Med. Image Anal.* 26 (1) (2015) 232–242.
- [56]. G. Azzopardi , N. Strisciuglio , M. Vento , N. Petkov , Trainable cosfire filters for vessel delineation with application to retinal images, *Med. Image Anal.* 19 (1) (2015) 46–57.
- [57]. J. Zhang , B. Dashtbozorg , E. Bekkers , J. Pluim , R. Duits , B. ter Haar Romeny ,Robust retinal vessel segmentation via locally adaptive derivative frames in orientation scores, *IEEE Trans. Med. Imaging* 35 (12) (2016) 2631–2644.
- [58]. K. Rezaee , J. Haddadnia , A. Tashk , Optimized clinical segmentation of retinal blood vessels by using combination of adaptive filtering, fuzzy entropy and skeletonization, *Appl. Soft Comput.* 52 (2017) 937–951.
- [59]. X. You , Q. Peng , Y. Yuan , Y.M. Cheung , J. Lei ,Segmentation of retinal blood vessels using the radial projection and semi-supervised approach, *Pattern Recognition*. 44 (10) (2011) 2314–2324.
- [60]. D. Marín , A. Aquino , M.E. Gegúndez-Arias , J.M. Bravo , A new supervised method for blood vessel segmentation in retinal images by using gray-level and moment invariants-based features, *IEEE Trans. Med. Imaging* 30 (1) (2011) 146–158.
- [61]. M.M. Fraz , P. Remagnino , A. Hoppe , B. Uyyanonvara , A.R. Rudnicka , C.G. Owen , S. Barman , An ensemble classification-based approach applied to retinal blood vessel segmentation, *IEEE Trans. Biomed. Eng.* 59 (9) (2012) 2538–2548.
- [62]. S. Roychowdhury , D. Koozekanani , K. Parhi , Blood vessel segmentation of fundus images by major vessel extraction and sub-image classification, *IEEE J. Biomed. Health Inform.* 19 (3) (2015) 1118–1128.
- [63]. R. Vega , G. Sanchez-Ante , L.E. Falcon-Morales , H. Sossa , E. Guevara , Retinal vessel extraction using lattice neural networks with dendritic processing, *Comput. Biol. Med.* 58 (2015) 20–30.
- [64]. Q. Li , B. Feng , L. Xie , P. Liang , H. Zhang , T. Wang , A cross-modality learning approach for vessel segmentation in retinal images, *IEEE Trans. Med. Imaging* 35 (1) (2016) 109–118.
- [65]. P. Liskowski , K. Krawiec , Segmenting retinal blood vessels with deep neural networks, *IEEE Trans. Med. Imaging* 35 (11) (2016) 2369–2380.
- [66]. B. Barkana , I. Saricicek , B. Yildirim , Performance analysis of descriptive statistical features in retinal vessel segmentation via fuzzy logic, ann, svm, and classifier fusion, *Knowl. Based Syst.* 118 (2017) 165–176.
- [67]. J. Zhang , Y. Chen , E. Bekkers , M. Wang , B. Dashtbozorg , B. ter Haar Romeny , Retinal vessel delineation using a brain-inspired wavelet transform and random forest, *Pattern Recognition*. 69 (2017) 107–123.
- [68]. C. Wang, Z. Zhao, Q. Ren, Y. Xu, and Y. Yu, “Dense u-net based on patch-based learning for retinal vessel segmentation,” *Entropy*, vol. 21, no. 2, p. 168, 2019.
- [69]. T. A. Soomro, A. J. Afifi, J. Gao, O. Hellwich, L. Zheng, and M. Paul, “Strided fully convolutional neural network for boosting the sensitivity of retinal blood vessels segmentation,” *Expert Systems with Applications*, vol. 134, pp. 36–52, 2019.